

## **New method for preparation of delivery systems of poorly soluble drugs on the basis of functionalized mesoporous MCM-41 nanoparticles**

M. Popova<sup>a,\*</sup>, A. Szegedi<sup>b</sup>, K. Yoncheva<sup>c</sup>, S. Konstantinov<sup>c</sup>, G.P. Petrova<sup>d</sup>, H.A. Aleksandrov<sup>d</sup>, G.N. Vayssilov<sup>d</sup>, P. Shestakova<sup>a</sup>

<sup>a</sup> Institute of Organic Chemistry with Centre of Phytochemistry, Bulgarian Academy of Sciences, 1113 Sofia, Bulgaria

<sup>b</sup> Research Centre for Natural Sciences, Institute of Materials and Environmental Chemistry, Hungarian Academy of Sciences, Magyar tudósok körútja 2, 1025 Budapest, Hungary

<sup>c</sup> Faculty of Pharmacy, Medical University of Sofia, 2 Dunav Str., 1000 Sofia, Bulgaria

<sup>d</sup> Faculty of Chemistry and Pharmacy, University of Sofia, 1126 Sofia, Bulgaria

### **A b s t r a c t**

MCM-41 silica with spherical morphology and small particle sizes (100 nm) was synthesized and modified by post-synthesis method with amino and/or carboxylic groups. Solid state reaction was applied for the first time for loading of poorly soluble drug mesalazine (5-aminosalicylic acid – 5-ASA). Thenon-loaded and drug loaded mesoporous silicas were characterized by XRD, TEM, N<sub>2</sub> physisorption, elemental analysis, thermal analysis, FT-IR and solid state NMR spectroscopy. Quantum-chemical calculations were used to predict the interactions between the drug molecule and the functional groups of the carrier. The nanoparticles were post-coated with sodium alginate and the coating modified the rate of mesalazine release from MCM-41NH<sub>2</sub> and MCM-41NH<sub>2</sub>COOH particles. Cytotoxic evaluation on colon adenocarcinoma cell line revealed that the alginate coating reduced cytotoxicity of mesalazine loaded in the post-coated particles compared to the pure mesalazine. The functionalized, polymer coated mesoporous systems are suitable oral drug delivery systems providing an opportunity to modify drug release.

### **1. Introduction**

Mesoporous silicas are promising materials for various aspects of biomedical applications. The preparation of mesoporous silica delivery systems of drugs and bioactive molecules is based on the advantages of mesoporous materials – tunable pore size, controlled particle size and morphology, and dual-functional surface (external and internal) [1–10]. The appropriate chemical surface modification of the mesoporous matrix is essential because the mesoporous silica surface covered with silanol groups is not selective enough to adsorb drug molecules with different functionalities [11–15]. Organophil surface modification can enhance the adsorption capacity of drug molecules, and it should also allow modulating their release. Modification of MCM-41 by different organic groups (chloropropyl, phenyl, benzyl, mercaptopropyl, cyanopropyl, butyl groups) resulted in higher ibuprofen loading and the ibuprofen release is slowed down with SH-Pr and NH<sub>2</sub>-Pr groups [4].

Amine-functionalized spherical MCM-41 with particle size of 490–770 nm show increased loading capacity (by about 10%) and slower drug release kinetics [7]. An optimal storage and release rate of ibuprofen probe molecule could be achieved by the functionalization of the mesoporous materials with appropriate amount of amino groups. The modification by 3-

amino-propyltriethoxysilane (APTES) can be accomplished in different solvents (toluene, ethanol etc.), at different temperatures and reaction times [3,5]. They can affect the amount and the distribution of functional groups [15–23]. The degree of drug loading depends on the specific surface area, the pore diameter of the carrier and the applied solvent for the loading process [4,18]. Moreover, their application as drug carriers can solve some problems associated with low stability and poor bioavailability of drug molecules.

Mesalazine (5-aminosalicylic acid – 5-ASA) is an antiinflammatory drug with low solubility and light sensitivity, which makes the preparation of a delivery system with it a difficult task [24]. The development of an appropriate method for its loading in nanosized mesoporous systems can stabilize and can enhance its bioavailability.

In the present work, solid state reaction is applied for the loading of mesalazine in mesoporous MCM-41 silicas functionalized by amino and by amino and carboxylic groups. Alginate coating of the mesalazine loaded MCM-41NH<sub>2</sub>COOH was applied in order to modify the release properties of the obtained delivery system.

## 2. Experimental

### 2.1. Synthesis of spherical MCM-41 silica material

MCM-41 with 100 nm particle size was prepared according to the procedure of Huh et al. [6]. This sol–gel procedure is carried out at 80°C without co-solvent, only in water solution and applying NaOH as a catalyst. The relative molar composition of the reaction mixture was: 1 TEOS:0.12 C16TMABr:0.31 NaOH:1190 H<sub>2</sub>O. The formed gel was aged at 80°C for 2 h, than washed with distilled water until neutral pH, and dried at ambient temperature. Template removal of MCM-41 materials was carried out in air (100 cm<sup>3</sup>/min) at 550°C with 1°C/min rate for 5 h.

### 2.2. Functionalization of the spherical MCM-41 by amino and/or carboxylic groups

Modification of the spherical MCM-41 with amino groups was accomplished by reaction with 3-amino-propyltriethoxysilane (APTES) in ethanol (5 h, 50°C) and in anhydrous toluene (24 h, 60°C), respectively. Samples were washed with several portions of solvent, and finally with water and dried at room temperature. The reaction of amino modified silicas with succinic anhydride was carried out in toluene. The amount of the applied succinic anhydride was calculated in order to transform 2/3 of amino groups to carboxylic groups. To remove adsorbed water azeotropic drying of amino modified silicas was made at 115°C by mixing 1 g of silica with 20 ml of anhydrous toluene. 6.6 mmol of succinic anhydride (assuming 2 wt.% of amino content on silica) was added to the mixture at 60°C and treated for 24 h. The samples were dried by vacuum evaporation (0.04 Pa) at room temperature for 6 h.

The parent mesoporous spherical silica material was designated as MCM-41, the amino and carboxylic modified ones as MCM-41NH<sub>2</sub> and MCM-41NH<sub>2</sub>COOH, respectively.

### 2.3. Mesalazine loading and nanoparticle post-coating

Powdered nanosized samples were loaded with mesalazine by solid state reaction. A 1:1 (by weight) ratio of mesalazine to solid sample was used. Mesalazine was mixed with the carriers at room temperature in a DDR-GM 9458 type high energy, vibrating ball mill for 3 min. Post-coating was performed by incubation of pre-formed mesoporous silica nanoparticles into aqueous phase containing 0.1 wt.% (by weight) sodium alginate under gentle stirring (100 rpm) for 2 h. After incubation, the dispersions were centrifuged at 15,000 rpm for 15 min,

rinsed with distilled water, separated by a second centrifugation, and finely dried at room temperature under vacuum.

#### 2.4. Characterization

X-ray powder diffraction patterns were recorded by a Philips PW 1810/3710 diffractometer with Bragg–Brentano parafocusing geometry applying monochromatized CuK $\alpha$  ( $k = 0.15418$  nm) radiation (40 kV, 35 mA) and proportional counter.

Nitrogen physisorption measurements were carried out at  $-196^{\circ}\text{C}$  using Quantachrome Autosorb 1C apparatus. The specific surface area was calculated by the BET method in the range of relative pressures from 0.02 to 1.0. The pore-size distribution was calculated from desorption branch of the isotherms with the BJH method. Silica samples were pre-treated at  $350^{\circ}\text{C}$ , whereas surface modified or drug loaded materials at  $80^{\circ}\text{C}$  for 5 h before measurements.

TEM images were taken using a MORGAGNI 268D TEM (100 kV; W filament; point-resolution = 0.5 nm). Samples were suspended in small amount of ethanol and a drop of suspension was deposited onto copper grid covered by carbon supporting film and dried at ambient.

Thermogravimetric measurements were performed with a Setaram TG92 instrument with a heating rate of  $5^{\circ}\text{C}/\text{min}$  in air flow.

Attenuated Total Reflection Infrared (ATR-FT-IR) spectra were recorded by means of a Varian Scimitar 2000 FT-IR spectrometer equipped with a MCT (mercury–cadmium–tellur) detector and a single reflection ATR unit (SPECAC “Golden Gate”) with diamond ATR element. In general, 128 scans and  $4\text{ cm}^{-1}$  resolution was applied. For all spectra ATR-correction was performed (Varian ResPro 4.0 software).

All NMR spectra were recorded on a Bruker Avance II+ 600 NMR spectrometer operating at 600.13 MHz proton frequency (150.90 MHz for  $^{13}\text{C}$ , 119.22 MHz for  $^{29}\text{Si}$ ), using 4 mm solid state CP/MAS dual probehead. The samples were loaded in 4 mm zirconia rotors and spun at magic angle spinning (MAS) rate of 6 kHz for  $^{13}\text{C}$  and 11 kHz for  $^{29}\text{Si}$  measurements.  $^{13}\text{C}$  NMR spectra were acquired with 8 K time domain data points, spectrum width of 50 kHz, 256 scans and a recycle delay of 5 s, using a cross polarization pulse sequence with total suppression of sidebands (cptoss) from Bruker Topspin library. The spectra were processed with an exponential window function (line broadening factor 10) and zero filled to 16 K data points. The  $^{29}\text{Si}$  NMR spectra were recorded with one-pulse sequence, 8 K time domain data points, spectrum width of 30 kHz, 3000–5000 scans and a relaxation delay of 10 s. Exponential window function was applied (line broadening factor 50) prior to Fourier transformation.

All ab initio molecular orbital calculations are performed with the Gaussian09 program suite [25] at M06-2x/6-311++G\*\* level [26,27] in the gas phase. All relative energies (in  $\text{kJ mol}^{-1}$ ) are calculated with respect to the most stable monomer structure of mesalazine (5-ASA\_01) and acetic acid/methyl amine molecule, representing  $-\text{COOH}$  and  $-\text{NH}_2$  groups in modified MCM-41.

#### 2.5. In vitro release study

In vitro drug release study was performed into acid buffer (0.1 N HCl,  $\text{pH} = 1.2$ ) and phosphate buffer ( $\text{pH} = 6.8$ ) at  $37^{\circ}\text{C}$ , under stirring at a rate of 100 rpm. 2.5 mg of the drug-loaded particles were incubated in 50 ml  $\text{pH} = 1.2$  or 6.8 at  $37^{\circ}\text{C}$  under stirring (100 rpm). At appropriate time intervals, 3 ml samples were withdrawn from the release medium (acid or phosphate buffer) and analyzed with UV–Vis spectroscopy at a wavelength of 302 or 330 nm,

respectively. The concentration of the released mesalazine was calculated according to the standard curves prepared in both media ( $r > 0.9993$ ).

### 2.6. *In vitro* cytotoxicity study

HT-29 cells (human colon adenocarcinoma cell line) were obtained from the German Collection of Microorganisms and Cell Cultures (DSMZ GmbH, Braunschweig, Germany). The cell viability after exposure to free mesalazine and mesalazine loaded nanoparticles was examined applying the MTT-dye reduction assay. Exponentially growing cells were seeded in 96-well flat-bottomed microplates (100  $\mu\text{L}$ /well) at a density of  $1 \times 10^5$  cells per mL and after a 24 h incubation at  $37^\circ\text{C}$  they were treated with graded concentrations of the samples. The incubation after the treatment was 72 h. After the exposure period 10  $\mu\text{L}$  MTT solution (10  $\text{mg mL}^{-1}$  in PBS) aliquots were added to each well. The microplates were further incubated for 4 h at  $37^\circ\text{C}$  and the formed MTT formazan crystals were dissolved through addition of 100  $\mu\text{L}$ /well 5% formic acid in 2-propanol. The MTT formazan absorption was determined using a microprocessor controlled microplate reader (Labexim LMR-1) at 580 nm.

## 3. Results and discussion

### 3.1. Material characterization

XRD data of the parent MCM-41 sample with the intense (100) and higher Miller indices reflections in the low 2 theta region confirm the formation of the hexagonal structure (not shown). However, decreased intensity and some broadened reflections are observed for the functionalized, mesalazine loaded mesoporous samples, indicating some structural disorder (Fig. 1). Also, the presence of crystalline mesalazine phase is registered on the MCM-41, MCM-41NH<sub>2</sub> and MCM-41NH<sub>2</sub>COOH samples. This is an evidence that a part of mesalazine can be found on the outer surface of the small spherical particles or in the secondary mesopores, e.g. in the voids among the particles.

Nitrogen adsorption and desorption isotherms of the parent, functionalized and mesalazine loaded samples are presented in Fig. 2. The calculated textural parameters for all samples are presented in Table 1. The isotherms of the parent and the amino modified MCM-41 exhibit a sharp increase at a relative pressure between  $p/p_0 = 0.2-0.4$ , which is associated with capillary condensation of nitrogen in the channels, and also an indication of narrow pore size distribution (Fig. 2). The two step modification procedure resulted in a significant specific surface area decrease for MCM-41NH<sub>2</sub>COOH. Also, narrower pore sizes were detected. The modification by amino and amino/carboxylic groups did not influence the spherical morphology of MCM-41 materials as evidenced by TEM investigations (Fig. 3).

The textural parameters of the functionalized MCM-41 samples loaded with mesalazine exhibits pore filling by interaction with mesalazine (Fig. 2 and Table 1). The adsorption of mesalazine on the parent and functionalized MCM-41 samples is related to extreme decrease of specific surface area, because of the total pore filling of the disordered pore structure.

ATR FT-IR method was used to investigate the interaction between the mesalazine molecule and the modified MCM-41 carriers after its deposition. The presence of amino and carboxylic groups was evidenced by ATR FT-IR measurements (Fig. 4). The FT-IR spectrum of mesalazine shows stretching vibration bands characteristic of carboxylate ( $-\text{COO}^-$ ) groups at 1573, 1445 and 1350  $\text{cm}^{-1}$  and a band at 1555  $\text{cm}^{-1}$  which can be attributed to the protonated form of amino groups, e.g.  $-\text{NH}_3^+$  [3,11–13]. The FT-IR spectra of MCM-41NH<sub>2</sub>Mes and MCM-41NH<sub>2</sub>COOHMes samples are similar to those of the pure mesalazine indicating no

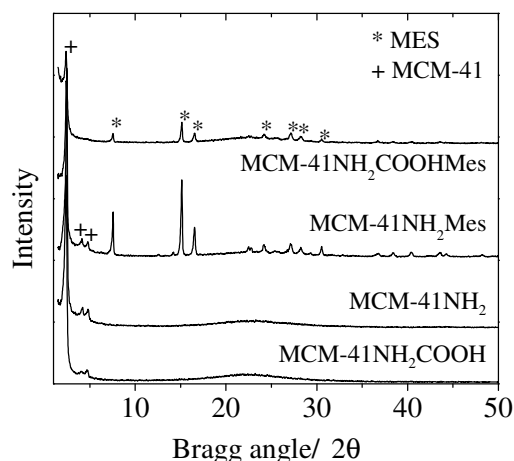


**Fig. 1.** XRD patterns of MCM-41NH<sub>2</sub> and MCM-41NH<sub>2</sub>COOH samples and their mesalazine loaded formulations

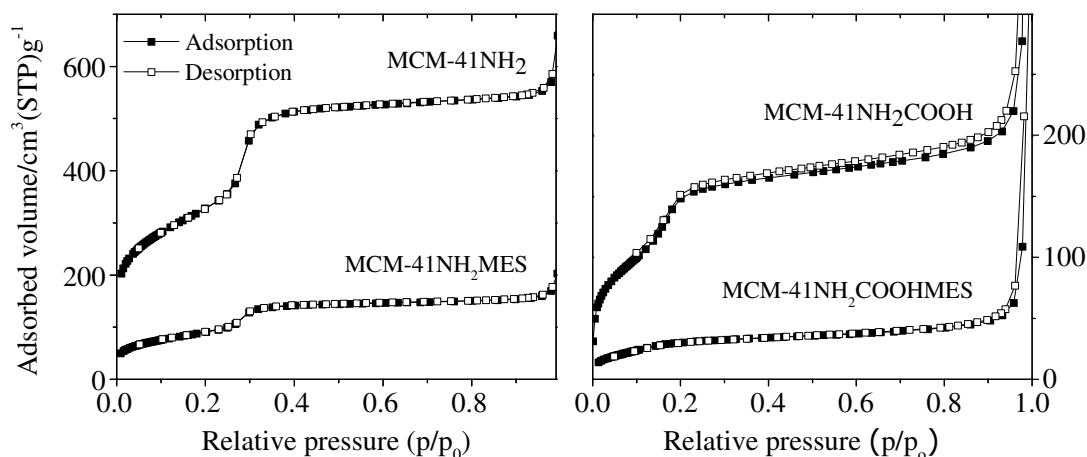


**Fig. 2.** N<sub>2</sub> adsorption–desorption isotherms of the parent and mesalazine-loaded MCM-41NH<sub>2</sub> and MCM-41NH<sub>2</sub>COOH samples.

**Table 1**

Physicochemical properties of the parent, functionalized, mesalazine loaded and alginate coated spherical MCM-41 samples.

Samples	$a_0^a$ (nm)	BET (m <sup>2</sup> /g)	PD <sup>b</sup> (nm)	Pore volume (cm <sup>3</sup> /g)
MCM-41	4.3	1175	2.7	0.97
MCM-41Mes	4.3	227	2.6	0.22
MCM-41NH <sub>2</sub>	4.2	1152	2.52	0.88
MCM-41NH <sub>2</sub> Mes	4.2	315	2.52	0.26
MCM-41NH <sub>2</sub> MesAlg	4.2	-	-	-
MCM-41NH <sub>2</sub> COOH	4.1	473	1.96	0.33
MCM-41NH <sub>2</sub> COOHMes	4.1	50	n.d.	0.07
MCM-41NH <sub>2</sub> COOHMesAlg	4.1	-	-	-

<sup>a</sup> cell parameter ( $a_0=2d_{100}(3)^{-1/2}$ ), <sup>b</sup> Pore diameter and pore volume calculated by BJH method, <sup>c</sup> calculated from UV absorbance analysis.

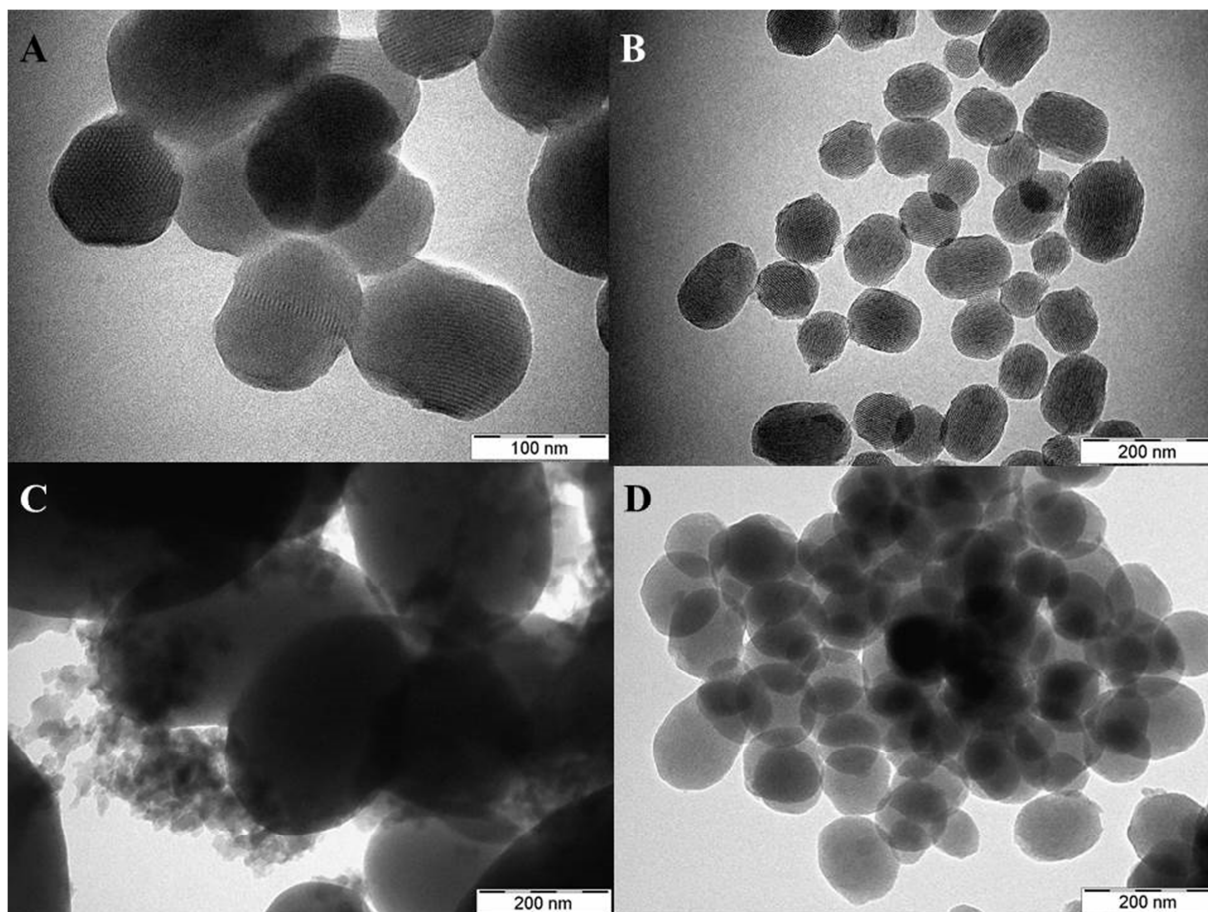


**Fig. 3.** TEM images of the parent MCM-41 (A and B), MCM-41NH<sub>2</sub> (C) and MCM-41NH<sub>2</sub>COOH (D) samples.

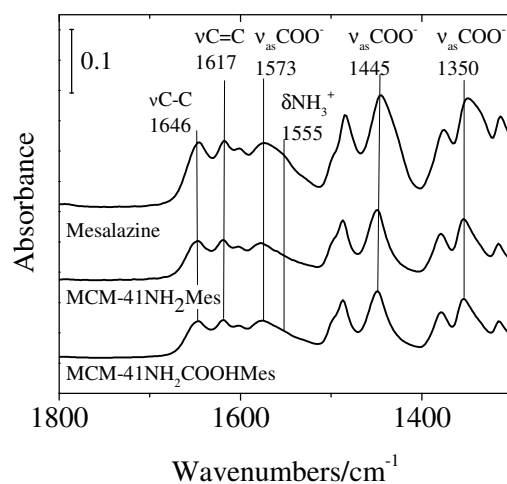


**Fig. 4.** FT-IR spectra of mesalazine loaded by solid-state method on MCM-41NH<sub>2</sub> and MCM-41NH<sub>2</sub>COOH.

interaction between the functionalized carriers and the mesalazine molecule. Despite the fact that nitrogen physisorption data show that mesalazine is confined in the pores, it seems that it cannot react with the functional groups. The incorporation of organic functional groups (NH<sub>2</sub> or NH<sub>2</sub>/COOH) was investigated by <sup>29</sup>Si NMR (Fig. 5). In the spectra of the modified

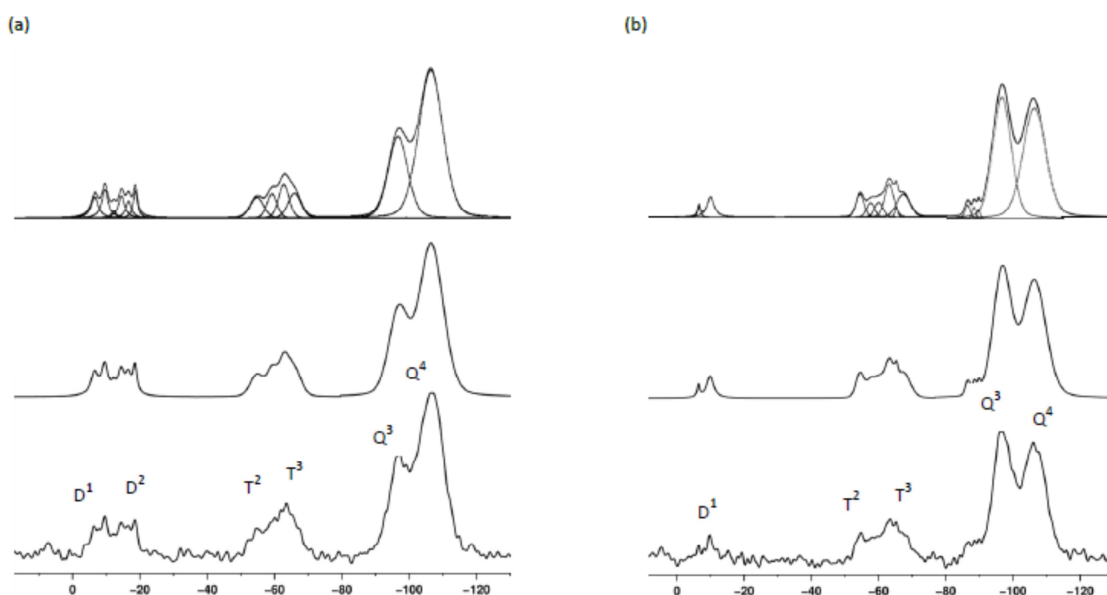
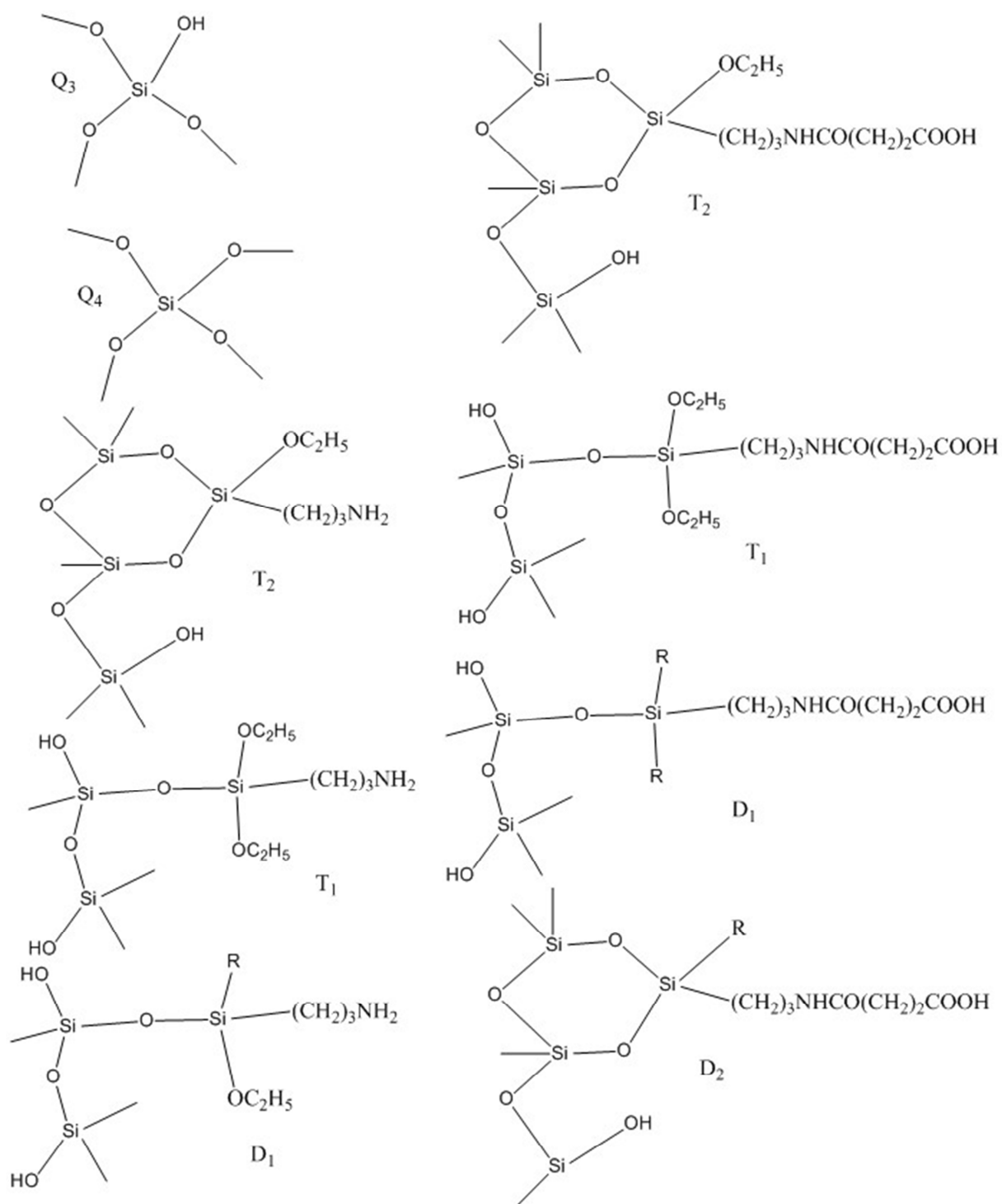


**Fig. 5.**  $^{29}\text{Si}$  NMR spectra of MCM-41NH<sub>2</sub>COOH (a) and MCM-41NH<sub>2</sub> (b). From bottom to top: experimental spectra, simulated spectra representing the sum of the deconvoluted spectral patterns and individual lines as result of spectra deconvolution.

samples three peaks are registered, at -106, -96 and -89 ppm (Fig. 4), which can be ascribed to Q<sup>4</sup>, Q<sup>3</sup> and Q<sup>2</sup> species [4,17] of the silica framework [Q<sup>n</sup> = Si(OSi)<sub>n</sub>(OH)<sub>4-n</sub>, n = 2–4] (Scheme 1). A broad, low intensity spectral pattern in the chemical shift region from -53 to -66 ppm typical for organosiloxane moieties is also observed, showing the presence of T<sup>2</sup>[(SiO)<sub>2</sub>Si-(R<sup>1</sup>)-OR<sup>2</sup>] (-55 ppm) and T<sup>3</sup> [(SiO)<sub>3</sub>Si-R<sup>1</sup>] (-65 ppm) species (Scheme 1) [4,17,28,29] respectively (Fig. 5, R<sup>1</sup> = (CH<sub>2</sub>)<sub>3</sub>NH<sub>2</sub> or (CH<sub>2</sub>)<sub>3</sub>NH<sub>2</sub>NHCO(CH<sub>2</sub>)<sub>2</sub>COOH; R<sup>2</sup> = CH<sub>2</sub>CH<sub>3</sub>). The appearance of the T<sup>2</sup> and T<sup>3</sup> peaks is an indication for the successful modification.

The  $^{29}\text{Si}$  spectra also display signals in the region between -6 and -19 ppm characteristic for D<sup>1</sup> and D<sup>2</sup> species [30]. The presence of these signals indicates that the incorporation of the organic linker is accompanied by disruption of the silica mesoporous structure. This process is more pronounced in MCM-41NH<sub>2</sub>COOH material since the amount of D<sup>1</sup> and D<sup>2</sup> species is higher as evidenced by its  $^{29}\text{Si}$  spectrum (Fig. 5).  $^{29}\text{Si}$  spectra of MCM-41NH<sub>2</sub> and MCM-41NH<sub>2</sub>COOH were subjected to deconvolution in order to quantitatively analyze the relative fractions of the different species formed in the functionalization process (Fig. 5). Data are summarized in Table 2. The T/(T+Q) ratio is a quantitative measure of the functionalization level in the modified silica materials. Calculations show that the modification is equally successful in both cases, however the fraction of D<sup>1</sup> and D<sup>2</sup> species is much higher in MCM-41NH<sub>2</sub>COOH material. The larger extent of silica framework deterioration in MCM-41NH<sub>2</sub>COOH material is also in agreement with the observed much lower BET surface area compared to MCM-41NH<sub>2</sub>.

The  $^{13}\text{C}$  NMR spectra of MCM-41NH<sub>2</sub> and MCM-41NH<sub>2</sub>COOH loaded with mesalazine are compared with the spectrum of pure mesalazine (Supplementary data). No chemical shift changes of the mesalazine carboxylic group signal (175 ppm) can be observed in the spectra. These results also support that there is no interaction between the drug molecules and the carrier and are in good accordance with FT-IR results.



**Scheme 1.** Structure of different silicon-containing moieties presented on the MCM-41NH<sub>2</sub> and MCM-41NH<sub>2</sub>COOH silicas.

**Table 2**

<sup>29</sup>Si NMR data for the functionalized samples.

Samples	Q <sup>4</sup>	Q <sup>3</sup>	Q <sup>2</sup>	T <sup>3</sup>	T <sup>2</sup>	D <sup>2</sup>	D <sup>1</sup>	T/(Q+T)	D/(Q+D)
MCM-41NH <sub>2</sub>	40.3	35.5	2.3	14.8	3.1		3.9	18.8	5.0
MCM-41NH <sub>2</sub> COOH	48.0	21.4	-	11.2	5.6	7.3	6.5	19.5	16.5

### 3.2. Quantum-chemical calculations

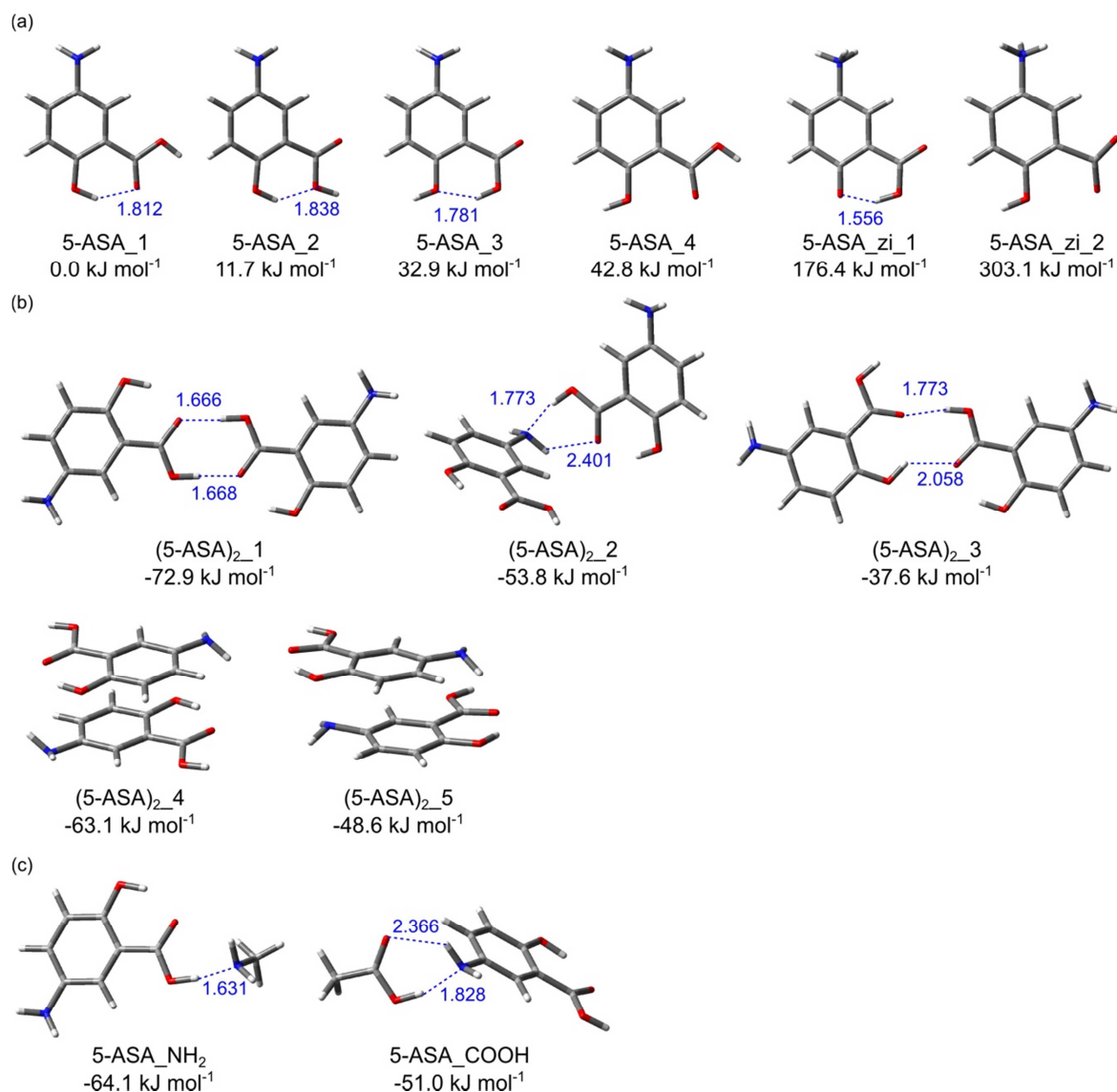


**Fig. 6.** Optimized structures of mesalazine monomers (a), dimers (b) and complexes with methylamine and acetic acid (c). Interatomic distances (in Å) represent H-bonds, energy values correspond to relative energy with respect to the most stable monomer structure 5-ASA\_1.

Quantum-chemical calculations were used to investigate the interaction between the drug molecule and the functional groups of the carrier. The optimized structures of the considered monomers and dimers of mesalazine (5-aminosalicylic acid – 5-ASA) as well as their relative energies and some important interatomic distances are presented in Fig. 6a and b, respectively. The structures of the complexes with methylamine and acetic acid used to mimic the interaction with the carrier functional groups are shown on panel c.

A detailed computational study of mesalazine molecular properties including IR spectrum, <sup>13</sup>C and <sup>1</sup>H NMR shifts, NBO charge distribution and electron density distribution and comparison with available experimental data was reported several years ago by Muthu et al. [31] at B3LYP/6-31G(d,p) level. Several structures of 5-ASA were optimized differing in the interaction between the hydroxyl group at ortho-position and the carboxylic group. The

structures are denoted as 5-ASA<sub>n</sub>, where the number n is assigned with respect to the stability of the structure. In the most stable conformer, 5-ASA<sub>1</sub>, strong H bond is formed between the hydroxyl H atom and the carbonyl oxygen with the interatomic distance estimated to 1.812 Å. Slightly less stable is the structure 5-ASA<sub>2</sub> with relative energy 11.7 kJ mol<sup>-1</sup>, in which the H-bond is formed with the hydroxyl oxygen of the carbonyl group and the interatomic [H–O] distance is longer by 0.026 Å. As can be expected, structures with hydroxyl group oriented opposite to the carboxylic group, 5-ASA<sub>3</sub> and 5-ASA<sub>4</sub>, are unstable with relative energies above 30 kJ mol<sup>-1</sup>.

The two zwitterion structures 5-ASA<sub>zi\_1</sub> with H-bond formed between the hydroxyl and the deprotonated carboxylic group and 5-ASA<sub>zi\_2</sub> without H-bond stabilization were found extremely unstable in gas phase with relative energies above 170 kJ mol<sup>-1</sup>. Such result is explained by the lack of stabilization effect of a polar solvent. Two types of dimer structures were considered: (i) dimers formed as a result of H-bond interaction between the different functional groups of the mesalazine molecule, and (ii) dimers formed as a result of  $\pi$ – $\pi$  stacking. The most stable dimer is (5-ASA)<sub>2\_1</sub> with H-bonds formed between the carboxylic groups of the individual molecules at distances ca. 1.67 Å, and interaction energy of -72.9 kJ mol<sup>-1</sup>. Formation of H-bonds involving the amine or hydroxyl groups of one molecule and the carboxyl group of the other, (5-ASA)<sub>2\_2</sub> and (5-ASA)<sub>2\_3</sub>, are less stable by 19.1 and 35.3 kJ mol<sup>-1</sup>, respectively, mainly due to the fact that such H-bonds are weaker. The  $\pi$ – $\pi$  dimer (5-ASA)<sub>2\_4</sub> is by less than 10 kJ mol<sup>-1</sup> less stable than (5-ASA)<sub>2\_1</sub> as for both  $\pi$ – $\pi$  dimers the distance between the molecules is estimated to ca. 3.1–3.3 Å.

At this stage of the study only the functional groups of the mesoporous carrier were considered in modeling the interaction of the mesalazine monomer with the carrier. The functional groups of the mesoporous carrier (amino and carboxylic) were represented as methylamine and acetic acid molecules, respectively (Fig. 6c). The interaction between the carboxylic group of 5-ASA and the amino group of the carrier is predicted to be stronger, since the relative energy of the complex 5-ASA<sub>NH<sub>2</sub></sub> is estimated to -64.1 kJ mol<sup>-1</sup> and the H-bond length in this case is only 1.631 Å. The complex 5-ASA<sub>COOH</sub> resembles to great extent the dimer structure (5-ASA)<sub>2\_2</sub>, forming a strong N{5-ASA}-H{carrier} bond with bond length 1.828 Å and a weaker one H{5-ASA}-O{carrier} at 2.366 Å. The relative energy of 5-ASA<sub>COOH</sub> is estimated to -51.0 kJ mol<sup>-1</sup>, i.e. by ca. 10 kJ mol<sup>-1</sup> less preferable than the 5-ASA<sub>NH<sub>2</sub></sub> structure. The interaction energies of the structures used for modeling of the mesalazine–carrier interactions, 5-ASA<sub>COOH</sub> and 5-ASA<sub>NH<sub>2</sub></sub>, are lower by 8.8 kJ mol<sup>-1</sup> (in absolute value) than the interaction energy between two mesalazine molecules. This may be the reason mesalazine molecules to remain bound between themselves but not coordinated to the functional groups of the carrier. These results are in good accordance with the FT-IR data (Fig. 4) and <sup>13</sup>C NMR spectra (Supplementary data 2).

### 3.3. Mesalazine loading and in vitro release

The functional groups, mesalazine and alginate content of the samples were quantified using thermogravimetric method. The amount of propylamino and aminopropyl/carboxylic groups connected on the surface of MCM-41 carrier was 10.7 wt.% and 19.6 wt.%, respectively (Fig. 7). The TG analysis determined the actual amount of drug in the carriers after correcting the curves by water and aminopropyl content for MCM-41NH<sub>2</sub>Mes and water, amino and carboxyl groups for MCM-41NH<sub>2</sub>COOHMes (Fig. 7). The weight losses from alginate layer of MCM-41NH<sub>2</sub>Mes and MCM-41NH<sub>2</sub>COOHMes was 7 wt% and 5 wt%, respectively (Fig. 7). The alginate content was calculated by correcting the actual weight loss with aminopropyl, carboxylic and mesalazine contents. In order to ensure the correct deduction of mesalazine amount, the concentration of the loaded mesalazine was checked by the eventual mesalazine

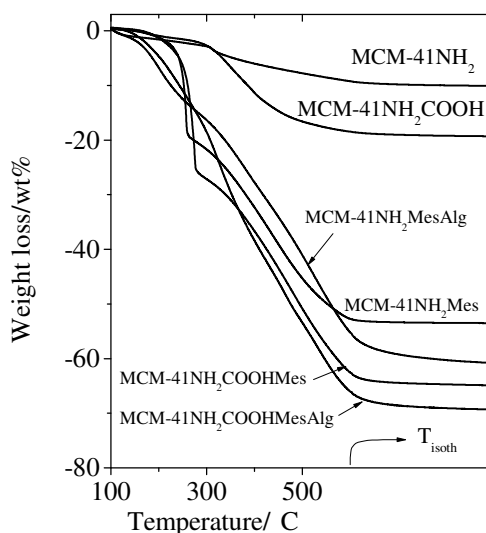


**Fig. 7.** TG profiles of mesalazine loaded MCM-41NH<sub>2</sub> and MCM-41NH<sub>2</sub>COOH and their alginate coated analogues.

loss during the coating procedure. Results showed that the amount of mesalazine after coating was the same as it was in non-coated samples, suggesting that mesalazine is not diffused out of the particles during the coating procedure. Drug release was faster from non-coated particles independent of their functionalization. In both buffers the release was completed in 1 h (Fig. 8). However, the process was slower after coating of the particles with sodium alginate. Significant decrease of the released drug amount was achieved in acid buffer that regarding physiological conditions suggested slow release of mesalazine in gastric fluid. This behavior was observed for both types of functionalized coated particles (MCM-41NH<sub>2</sub> and MCM-41NH<sub>2</sub>COOH) where approximately 15% of the drug was released for 2 h (Fig. 8). This is an important fact, taking into account that for the treatment of inflammatory bowel diseases mesalazine should be delivered at the higher pH of intestinal fluids. Moreover, the studies in buffer with a higher pH (6.8) showed faster release of mesalazine from coated particles compared to that of in acid buffer. In particular, 100% mesalazine was released from MCM-41NH<sub>2</sub>COOHAlg particles in 2 h, and approximately 60% from MCM-41NH<sub>2</sub>Alg particles for the same time. In both cases, the profiles showed that the release rate from the coated particles was slightly lower compared to non-coated ones. Therefore alginate coating reduced the initial burst release that is frequently observed for mesoporous silica particles. In addition, coating made possible to achieve specific delivery at the desired region of gastrointestinal tract, in the present case the small intestine.

### 3.4. Cytotoxicity study

The cytotoxicity of free mesalazine and mesalazine loaded nanoparticles was investigated in HT-29 cells, which monolayer cultures were used as colon mucosa model (Fig. 9). Our study revealed dose dependent cytotoxicity of free mesalazine correlating with previously reported data [32]. This indicates direct cell damage by free mesalazine even at the lowest applied concentration of 20 µg/ml. Such cytotoxicity may lead to mucositis, and therefore be at least in part responsible for the appearance of mesalazine frequent adverse drug reactions like diarrhea, stomach pain, nausea and vomiting. The incorporation of the drug into both functionalized mesoporous particles did not change this effect. However, the post-coating of nanoparticles with sodium alginate led to reduced cytotoxic effect of mesalazine even at the

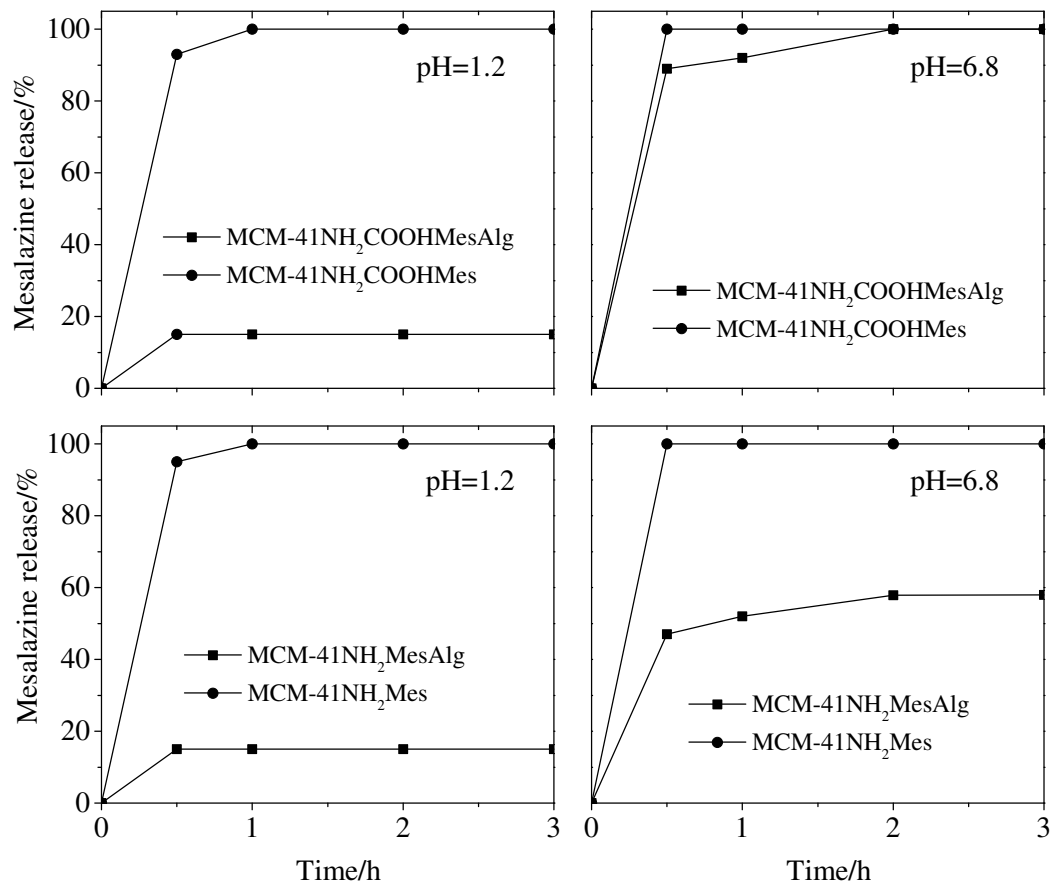


**Fig. 8.** Release profiles of mesalazine loaded MCM-41NH<sub>2</sub> and MCM-41NH<sub>2</sub>COOH and alginate coated drug delivery systems.

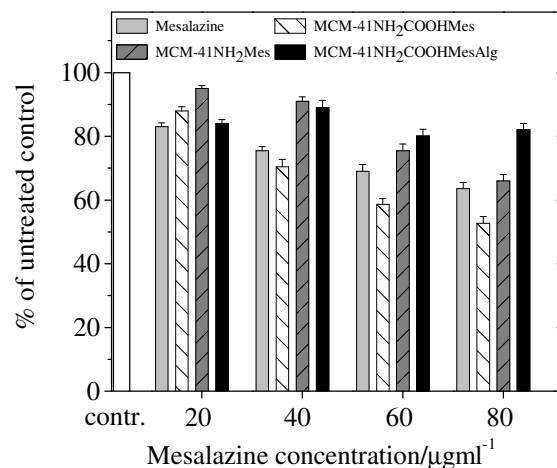


**Fig. 9.** In vitro cytotoxicity of mesalazine loaded MCM-41NH<sub>2</sub> and MCM-41NH<sub>2</sub>COOH samples and their alginate coated analogues on HT-29 cell lines.

highest concentration (80 μg/ml). Further experiments with cell culture and animal models of inflammatory bowel diseases such as ulcerative colitis and Crohn's disease could reveal the therapeutic efficacy of the polymer coated mesalazine delivery system.

## 4. Conclusions

MCM-41 silica with spherical morphology and small particle sizes (100 nm) was synthesized and modified by post-synthesis method with amino and amino/carboxylic groups. Mesalazine, a drug molecule with amino and carboxylic groups, can be successfully introduced into the channels of MCM-41 by solid-state reaction. Appropriate surface functionalization of silica particles provides the opportunity for further polymer coating. The postcoating of the bifunctional (amino and carboxylic) nanoparticles with sodium alginate revealed the capacity to achieve different drug release rates depending on the pH value of the release medium. In addition, reduction of the mucosal damage by mesalazine could be achieved after polymer coating of the nanoparticles.

## Acknowledgements

Financial support from the project BG051PO001-3.3.05-0001 “Наука и бизнес” (Д03-134/02.04.2014 (II-8-16)) and by the Bulgarian-Hungarian Inter-Academic Exchange Agreement is greatly acknowledged. G.P.P., H.A.A., and G.N.V. are grateful to the Bulgarian Science Fund (Grant DCVP 02/1) and the FP7 programme (project Beyond Everest).

## Appendix A. Supplementary data

Supplementary data associated with this article can be found, in the online version, at <http://dx.doi.org/10.1016/j.micromeso.2014.07.044>.

## References

- [1] F. Balas, M. Manzano, P. Horcajada, M. Vallet-Regi, *J. Am. Chem. Soc.* 128 (2006) 8116–8117.
- [2] V. Cauda, A. Schlossbauer, Th. Bein, *Microporous Mesoporous Mater.* 132 (2010) 60–71.
- [3] Q. He, J. Shi, F. Chen, M. Zhu, L. Zhang, *Biomaterials* 31 (2010) 3335–3346.
- [4] P. Horcajada, A. Ramila, G. Ferey, M. Vallet-Regi, *Solid State Sci.* 8 (2006) 1243–1249.
- [5] Y. Cho, R. Shi, R.B. Borgens, A. Ivanisevic, *Nanomedicine* 3 (2008) 507–519.
- [6] S. Huh, J.W. Wiench, J.-C.h. Yoo, M. Pruski, V.S.-Y. Lin, *Chem. Mater.* 15 (2003) 4247–4256.
- [7] M. Manzano, V. Aina, C.O. Arean, F. Balas, V. Cauda, M. Colilla, M.R. Delgado, M. Vallet-Regi, *Chem. Eng. J.* 137 (2008) 30–37.
- [8] I. Izquierdo-Barba, M. Colilla, M. Manzano, M. Vallet-Regi, *Microporous Mesoporous Mater.* 132 (2010) 442–452.
- [9] A. Katiyar, S. Yadav, P.G. Smirniotis, N.G. Pinto, *J. Chromatogr. A* 1122 (2006) 13–20.
- [10] Sh. Shen, P.Sh. Chow, S. Kim, K. Zhu, R.B.H. Tan, *J. Colloid Interface Sci.* 331 (2008) 365–371.
- [11] B. Munoz, A. Ramila, J.P. Pariente, I. Diaz, M.A. Vallet-Regi, *Chem. Mater.* 15 (2003) 500–503.
- [12] Q.L. Tang, Y. Xu, D. Wu, Y.H. Sun, J.Q. Wang, J. Xu, F. Deng, *J. Control. Rel.* 114 (2006) 41–46.
- [13] F.Y. Qu, G.S. Zhu, S.Y. Huang, S.G. Li, S.L. Qiu, *Chem. Phys. Chem.* 7 (2006) 400–406.
- [14] A. Szegedi, M. Popova, I. Goshev, J. Mihaly, *J. Solid State Chem.* 184 (2011)

1201–1207.

- [15] J.M. Rosenholm, C. Sahlgren, M. Linden, *Nanoscale* 2 (2010) 1870–1883.
- [16] B.G. Trewyn, I.I. Slowing, S. Giri, H.-T. Chen, V.S.-Y. Lin, *Acc. Chem. Res.* 40 (2007) 846–853.
- [17] Q.L. Tang, Y. Xu, D. Wu, Y.H. Sun, *J. Solid State Chem.* 179 (2006) 1513–1520.
- [18] Sh. Wang, *Microporous Mesoporous Mater.* 117 (2009) 1–9.
- [19] C.M. Yang, B. Zibrowius, F. Schuth, *Chem. Commun.* 14 (2003) 1772–1773. [20] Q. Yang, S.C. Wang, *Chem. Mater.* 17 (2005) 5999–6003.
- [21] M.A. Vallet-Regi, J. Perez-Pariente *Chem. Mater.* 13 (2001) 308–311.
- [22] M.A. Vallet-Regi, L. Ruiz-Gonzalez, *J. Mater. Chem.* 16 (2006) 26–31.
- [23] P. Yang, Z. Quan, L. Lu, Sh. Huang, J. Lin, *Biomaterials* 29 (2008) 692–702.
- [24] R.K. Singh, P.S. Patel, P. Gupta, *Int. J. Pharm. Sci. Res.* 1 (3) (2010) 44–49.
- [25] M.J. Frisch, G.W. Trucks, H.B. Schlegel, G.E. Scuseria, M.A. Robb, J.R. Cheeseman, J.A. Montgomery Jr., T. Vreven, K.N. Kudin, J.C. Burant, J.M. Millam, S.S. Iyengar, J. Tomasi, V. Barone, B. Mennucci, M. Cossi, G. Scalmani, N. Rega, G.A. Petersson, H. Nakatsuji, M. Hada, M. Ehara, K. Toyota, R. Fukuda, J. Hasegawa, M. Ishida, T. Nakajima, Y. Honda, O. Kitao, H. Nakai, M. Klene, X. Li, J.E. Knox, H.P. Hratchian, J.B. Cross, V. Bakken, C. Adamo, J. Jaramillo, R. Gomperts, R.E. Stratmann, O. Yazyev, A.J. Austin, R. Cammi, C. Pomelli, J.W. Ochterski, P.Y. Ayala, K. Morokuma, G.A. Voth, P. Salvador, J.J. Dannenberg, V.G. Zakrzewski, S. Dapprich, A.D. Daniels, M.C. Strain, O. Farkas, D.K. Malick, A.D. Rabuck, K. Raghavachari, J.B. Foresman, J.V. Ortiz, Q. Cui, A.G. Baboul, S. Clifford, J. Cioslowski, B.B. Stefanov, G. Liu, A. Liashenko, P. Piskorz, I. Komaromi, R.L. Martin, D.J. Fox, T. Keith, M.A. Al-Laham, C.Y. Peng, A. Nanayakkara, M. Challacombe, P.M.W. Gill, B. Johnson, W. Chen, M.W. Wong, C. Gonzalez, J.A. Pople, Gaussian 03, Revision E.01, Gaussian, Inc., Wallingford, CT, 2004.
- [26] Y. Zhao, D.G. Truhlar, *Theor. Chem. Acc.* 120 (2008) 215–241.
- [27] A.D. McLean, G.S.J. Chandler, *Chem. Phys.* 72 (1980) 5639–5648.
- [28] N. Garcia, E. Benito, J. Guzman, P. Tiemblo, V. Morales, R.A. Garcia, *Microporous Mesoporous Mater.* 106 (2007) 129–139.
- [29] T. Borrego, M. Andrade, M.L. Pinto, A. Rosa Silva, A.P. Carvalho, J. Rocha, C. Freire, J. Pires, *J. Colloid Interface Sci.* 344 (2010) 603–610.
- [30] R.H. Glaser, G.L. Wilkes, *J. Non-Cryst. Sol.* 113 (1989) 73–87.
- [31] S. Muthu, E.I. Paulraj, *J. Chem. Pharm. Res.* 3 (2011) 323–339.
- [32] E. Noble, L. Janssen, P.J. Dierickx, *Cell Biol. Toxicol.* 13 (1997) 445–451.